Proceedings of the Fifth International Conference

Remote Sensing for Marine and Coastal Environments

Volume II

5-7 October 1998
San Diego, California, USA

AIRBORNE LIDAR REMOTE SENSING OF COASTAL WAVES AND BREAKING DISTRIBUTION*

Paul A. Hwang[1], William B. Krabill[2], Wayne Wright[2],
Edward J. Walsh[2,4], and Robert N. Swift[3]
[1]Oceanography Division, Naval Research Laboratory, Stennis Space Center, MS
[2]NASA/GFSC Laboratory for Hydrospheric Processes, Wallops Island, VA
[3]EG&G Services, Inc., N159, Wallops Flight Facility, Wallops Island, VA
[4] Presently on assignment at NOAA Environmental Technology Laboratory, Boulder, CO

ABSTRACT

A scanning lidar system provides high-resolution two-dimensional measurements of ocean wave displacement. The airborne operation further enhances the speed of data acquisition. These properties allow rapid characterization of the ocean wave environment. In addition to active ranging, the scanning optics can obtain passive measurements of surface emissivity, yielding a digital image of the surface brightness "on the fly." Processed into a binary image, these measurements can provide information on the average statistics and the spatial distribution of breaking waves. Technical specifications of the system and examples of its application are presented.

1.0 INTRODUCTION

Laser ranging was introduced for airborne ocean wave measurement in the '70s (Schule et al. 1971; Hoge et al. 1980). Using the high-resolution profiling (one-dimensional) mode, Schule et al. (1971) obtained transect wavenumber spectrum in the wind direction to study the wave growth mechanism and the properties of wavenumber spectrum (see also discussions in Phillips 1977, Ch. 4). Since then, many improvements have been incorporated into the design of newer generations of airborne lidars. The most significant advances include the two-dimensional scanning capability (Krabill et al. 1995 a, b) and the correction of the aircraft motion using the kinematic global positioning system (GPS) technique (Krabill and Martin 1987). Although these improvements were supported mainly by the Greenland ice research, the technology is obviously also suitable for measuring the topography of ocean surface waves.

Most recently, a new capability was added to the system that uses the laser scanning optics in passive mode to collect a digital image of the ground or ocean surface. This latest addition is useful for analysiing the spatial distribution of breaking patches on the ocean surface. In addition to the lidar system, video images or 70 mm photographs are routinely collected during each airborne measurement mission. The combination of active ranging, passive imaging and continuous video recording of the ocean surface represents a powerful tool for the study of ocean wave dynamics on the continental shelf. In Section 2, we provide a brief description of the measurement system. Section 3 describes three data sets collected in two field experiments (Duck94 and SandyDuck97) organized by the Office of Naval Research and the U. S. Army Corps of Engineers (Birkemeier et al. 1994, 1996). Section 4 presents a few applications of using the airborne scanning lidar data in ocean wave research. Section 5 summarizes the paper with concluding remarks.

---

* Presented at the Fifth International Conference on Remote Sensing for Marine and Coastal Environments, San Diego, California, 5-7 October 1998.

2.0 MEASUREMENT SYSTEM

The key instrument of the ocean wave measurement system described in this paper is the airborne topographic mapper (ATM). This is an airborne scanning lidar ranging system originally designed for monitoring the annual variation of the Greenland ice sheet. The hardware design has been described elsewhere (Krabill et al. 1995 a, b). Here we only discuss briefly the scanning method and the technical specification of the vertical and horizontal resolutions.

The ATM measures the range between the aircraft and the surface of the ground or ocean. It uses a nutating scanning mirror to project the laser beam in a circular pattern on the surface with a 15° incident angle. Carried on a moving aircraft, the locus of the scanning pattern is approximately an oval shape with the major axis in the cross-track direction and the minor axis in the along-track direction. The repetition rate of the azimuthal scanning cycles is 10 Hz. The laser is pulsed at 5 kHz so there are 500 range measurements evenly spaced around each scan cycle. These are interlaced with 500 passive digital measurements of the surface emissivity. The operational altitude of the aircraft is typically between 400 to 600 m. With an 1 mrad dispersion angle of the laser beam, the footprint of the laser spot on the ocean surface is between 0.4 to 0.6 m. The swath of the image is between 200 to 300 m, and the spacing between neighboring active and passive image pixels is between 1.3 to 1.9 m. The vertical resolution of the ranging is dictated by the determination of the aircraft position. The theoretical accuracy of the kinematic GPS system is 0.01 to 0.02 m. Dynamic calibration of the GPS measurements and the laser ranging to a calm water body shows that the rms error of the vertical resolution is actually better than 0.1 m (Krabill and Martin 1987). A comparison of the surface wave topography derived by a scanning lidar and a 70 mm photograph of the ocean surface taken nearly simultaneously is shown in Hwang et al. (1998). The high-fidelity measurement of the ocean waves is quite evident. In the figure, the nonlinear features such as the narrow crests and the flattened troughs of these shoaling waves in the coastal region can be clearly identified in both sets of images. Other detailed features such as the distortion of the wave fronts and even the "scallops" of the coastline are faithfully captured.

For quantitative analyses of the wave data, the circular scanning data are resampled into rectangular grids. Because the data density is sparser near the central region than that near the two edges, the rectangular grid size is dictated by the spacing in the central region. This spacing is determined by the speed of the aircraft and the laser scan rate. Because the repetition rate of the scanning cycles is 10 Hz, the scanning arc advances every 0.1 s in the along track direction. The typical speed used in the wave mapping missions was either 60 or 100 m s^{-1} depending on the aircraft used, which translates to a grid size of 6 to 10 m along track. The cross track grid size can be maintained at the original scanning spacing (1.3 to 1.9 m).

3.0 DESCRIPTION OF FIELD EXPERIMENTS

The ATM system participated in Duck94 and SandyDuck97 and completed three flight missions. The width of the continental slope in the region is approximately 100 km. The bathymetric changes are relatively mild. The flight pattern in Duck94 included both along shore and cross shore tracks. Some of the tracks extended to more than 80 km offshore. During SandyDuck97, the aircraft flew a repeated racetrack pattern with two long tracks approximately perpendicular to the bathymetry contours. The seaward extent of the tracks is 40 km from the coastline. During Duck94, a NASA P3 aircraft was used. The flight speed varied from 90 to 105 m s^{-1}. The measurements were acquired on October 17 and 18, 1994, with a flight time of 2 and 3 hours, respectively. Prior to the flight, a major extratropical storm arrived in the area on October 15 and wind speed reached 20 m s^{-1} from North. The wind speed and wind direction were recorded by the anemometer installed at the end of the pier (approximately 600 m offshore) of the U. S. Army Field Research Facility (FRF). The relevant wind and wave conditions during

the experimental duration are shown in Figures 1. During the flight period on October 17, the wind had decreased to approximately 9 m s^{-1} from North (Figures 1a and 1b). The significant wave height measured by a wave buoy located 4 km offshore was approximately 2.1 m and the peak wave period was between 10 to 11 s (Figures 1c and d). On October 18, the wind further decreased to 0 to 3 m/s during the flight period. The wave height was approximately 1.9 m and the peak wave period was between 10.5 to 11.5 s (Figures 1c and d). In both missions, the wave systems were dominated by the swell generated by the earlier storm. The data represent a simple swell case (October 18) and wind waves on background swell (October 17).

During SandyDuck97, the aircraft (a NOAA Twin Otter) flew for 4 hours (from 7 AM to 11 AM EST) on September 24, 1997. A front had passed through the area the night before. Wind speed increased from 4 to 12 m s^{-1} within a two hour period (10:30 PM September 23 to 12:30 AM September 24) and wind direction shifted from westerly to northerly (Figures 2a and b). The wind speed was quasi-steady at approximately 9.5 m s^{-1} from 2 to 9 AM September 24, and then gradually decreased from 9.5 to 7.5 m s^{-1} during the second half of the mission. This front generated a new wave system with the significant wave height increasing rapidly from 0.5 to 1.2 m within 2 hours in response to the rapid increase in wind speed (Figure 2c). The peak wave period also increased from 2.5 to 5 s during the frontal passage (Figure 2d). For the first two hours of the flight (7 to 9 AM), the data represent active wind wave generation; and for the last two hours, they are typical of decaying wave field.

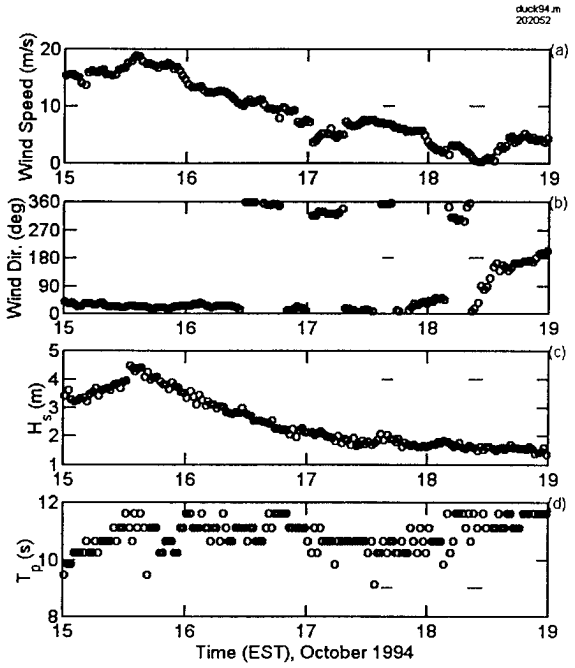

Figure 1. The Experimental Conditions Of (A) Wind Speed, (B) Wind Direction, (C) Significant Wave Height, And (D) Peak Wave Period During October 15 To 19, 1994 Of The Duck94 Experiment. The Short Line Segment On Each Plot Represents The Time Of Airborne Wave Measurements.

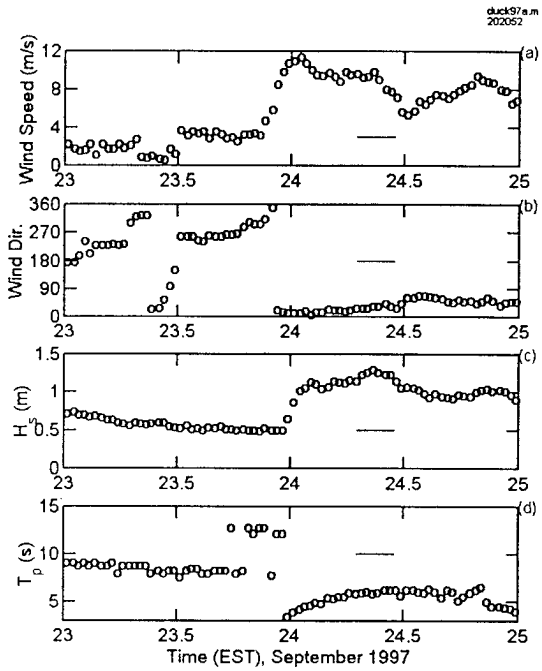

Figure 2. Same As Figure 1 But For The Period Of September 23 to 25, 19

The passive digital surface imaging capability was not available during the Duck94 experiment. Instead, contiguous 70 mm photographs were taken during the along-beach flight lines. In addition, a

scanning radar altimeter (SRA) was carried on the NASA P3. For SandyDuck97, video recording replaced 70 mm photographs and passive digital images from the scanner were also available. In the following section we present examples of the data to illustrate a few applications using these spatial and temporal measurements of the surface wave field.

4.0 WAVENUMBER SPECTRUM AND BREAKING DISTRIBUTION

4.1 WAVENUMBER SPECTRUM

The most obvious utilization of these two-dimensional measurements of the ocean surface topography is the direct computation of the vector wavenumber spectrum. Figure 3a shows a 20-s segment of the surface topography covering an area approximately 180 m × 1400 m. The data were collected on 9/24/97 starting at 09:35:11 AM. The resampled rectangular grid size is 6 m in the along track (x) direction and 3 m in the cross track (y) direction. The wave pattern can be easily identified. The two-dimensional wavenumber spectrum can be calculated using a standard 2-D FFT procedure. (The results presented in this paper are processed using MATLAB.) Figure 3b shows an example of the wavenumber spectrum computed from an image segment of 180 m × 200 m. Even with a small image of this size, the dominate wavelength and propagation direction are clearly identified in both the spatial plot and the wavenumber spectrum. This is an equivalent of 3 s flight data and illustrates the capability of rapid characterization of the surface wave properties using an airborne scanning lidar.

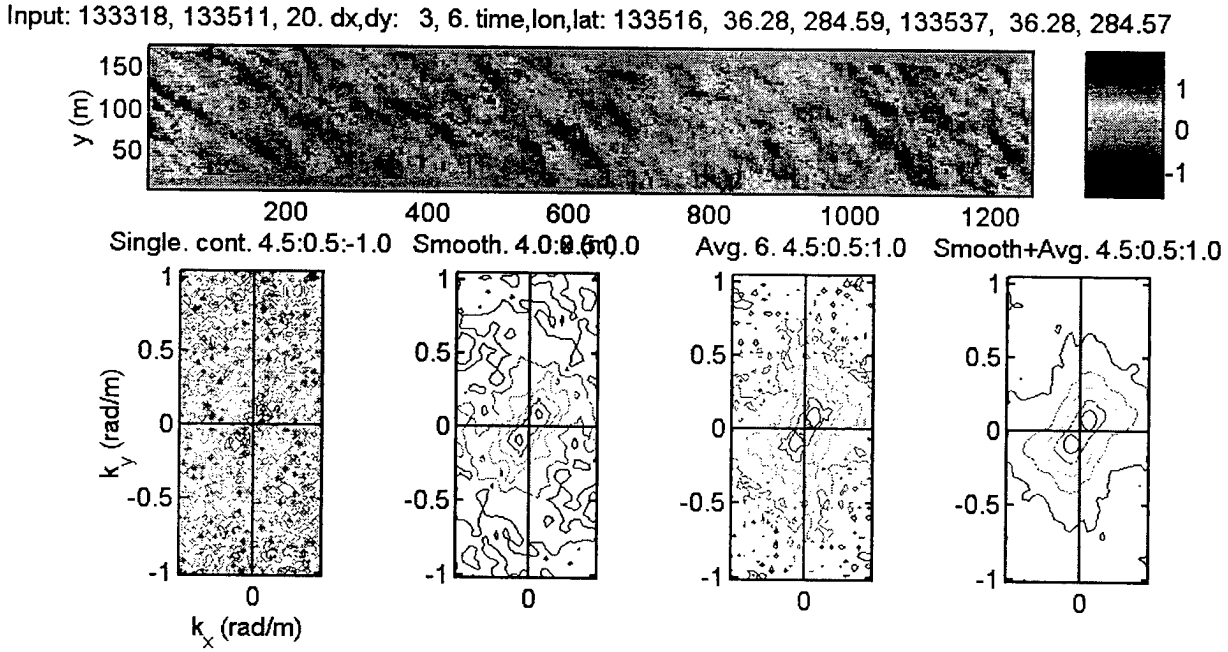

Figure 3. (a) A Segment Of The Two-Dimensional Surface Wave Topography. The Image Area Is Approximately 180 m × 1400 m. The Image Is Resampled From The Scanning Lidar Data And Reoriented In The Rectangular Coordinate System With Respect To The Flight Tract As The x-Direction. (b) A Two-Dimensional Wavenumber Spectrum Calculated From A Subsegment (180 m × 200 m) Of The Data Shown In (a). (c) The Result Of 3 × 3 Bin Averaging To Smooth The Wavenumber Spectrum Shown In (b). (d) The Ensemble Average Of 7 Spectra, Each Calculated From A Non-Overlapping Segment Of 180 m × 200 m Wave Field. (e) The 3 × 3 Bin Averaged Spectrum Of The Ensemble Averaged Spectrum Shown In (d).

One can apply ensemble averaging or bin averaging to increase the statistical confidence of the spectral estimate. Figure 3c is a smoothed spectrum of the one displayed in Figure 3b. The smoothing is over a 3×3 grid mask with a weighting function of 1/4 for the central cell, 1/8 for the four neighboring cells and 1/16 for the four corner cells. The degrees of freedom of the new spectrum are 18 as compared to 2 for the raw spectrum. The result of ensemble average of 7 consecutive image segments (14 degrees of freedom) is shown in Figure 3d. The spectrum obtained by both ensemble average (of 7) and bin average (of 9) is shown in Figure 3e, which results in a reasonably smooth spectrum. In either case, the spectral properties of the dominant waves are easily determined from the two-dimensional spatial measurement of the surface elevation.

The spectra plotted in Figures 3b-e represent the encounter spectra as observed from the moving aircraft. Due to the relative velocity of the aircraft and the wave propagation, the wavelength will appear longer when the aircraft moves in the direction of wave propagation, and shorter when it travels in the opposite direction. The fractional error in wavelength estimate is the ratio between the wave phase speed and the aircraft velocity. In addition to the relative motion of the aircraft and the wave field, any difference between the aircraft heading and the ground track orientation requires a drift angle correction in the resulting wavenumber spectrum. Walsh et al. (1985) present a detailed analysis and the correction procedures for the relative motion and the aircraft heading. Because these corrections are phase velocity dependent, the resulting wavenumber grids are no longer in equal spacing thus making graphic presentation rather difficult. We will not attempt to plot the two-dimensional spectrum in the corrected wavenumber space. In the present case, the phase speed of 6-s waves is 9 m s^{-1} and the speed of the aircraft is 60 m s^{-1}. The wavelength correction at the spectral peak is approximately 15 %. The corrected peak wavenumber of this wave field (Figure 3a) is 0.10 rad m^{-1} (the peak wavelength L_p=61 m). The propagation direction is approximately 40° with respect to the flight track, which is almost perpendicular to the coastline. These are consistent to the buoy measurements (at 900 m offshore) of the significant wave height (1.30 m), peak wave period (6.5±0.5 s, corresponding to L_p=66±10 m), and the northeasterly wind direction that generated this wave system.

4.2 DISTRIBUTIONS OF BREAKING PATCHES

As discussed earlier, when the laser is on, the ATM produces active ranging of the distance between the aircraft and the ocean surface. When the laser is off, the ATM optics receives a reading of the surface brightness. This is equivalent to digitizing the picture of the ocean surface "on the fly." One application of these digital surface images is the discrimination of breaking patches from the background water surface. The intensity contract between the foam produced by breaking events and the background sea water is very high. Thus a digital picture of the ocean surface can be properly thresholded to create a binary image of the ocean surface. (During the experimental period, there was an overcast in the sky and no Sun glint appeared in the images.) Statistical analysis indicates that the intensity distribution is gaussian-like. The mean and the standard deviation of the passive intensity data are calculated. The threshold is then set at a level corresponding to several standard deviations above the mean. At this stage, the determination of the multiplication factor for the threshold is empirical. A limited number of tests suggest that the magnitude of the multiplication factor to be between 2 and 4. Figure 4 shows two binary images of the ocean surface brightness with thresholds set at 2.5 and 3.5 standard deviations above the mean. The two solid lines on each plot indicate the swath boundaries of the measurements. This is the same region as that of Figure 3a, but plotted in the longitude and latitude coordinates. The region is approximately 35 km offshore at 30 m water depth. The time of the data acquisition was 09:35:16 to 09:35:36, September 24, 1997. The wind speed measured by the nearshore station at the pier end was about 9 m s^{-1}. The breaking percentage (here defined as the percentage of the water surface that appears brighter than the threshold) can be calculated from the binary images. For the two thresholds used in Figure 4, the fraction of breaking surface is found

to be 0.0063 and 0.0020, respectively.

The quantitative observation of wave breaking events has been a difficult task. The data based on the measurements of whitecap coverage (e.g., Monahan 1971; Monahan and O'Muircheartaigh 1980) typically show an order of magnitude scatter (see, e.g., the data compiled in Wu 1988, Figures 1 and 2). The formula proposed by Wu (1988) for the whitecap coverage is

$$W = 1.7 \times 10^{-6} U^{3.75} \tag{1}$$

where W is the whitecap coverage and U is the reference wind speed at 10 m elevation. For the 9 m s^{-1} wind speed, the calculated whitecap coverage is 0.0064, in good agreement with the present processing of the passive binary image with a threshold of 2.5 times the standard deviation. The technique is promising for the study of breaking statistics in the ocean. The empirical threshold can also be compared with the corresponding measurements from video recording for further validation. This verification remains to be done.

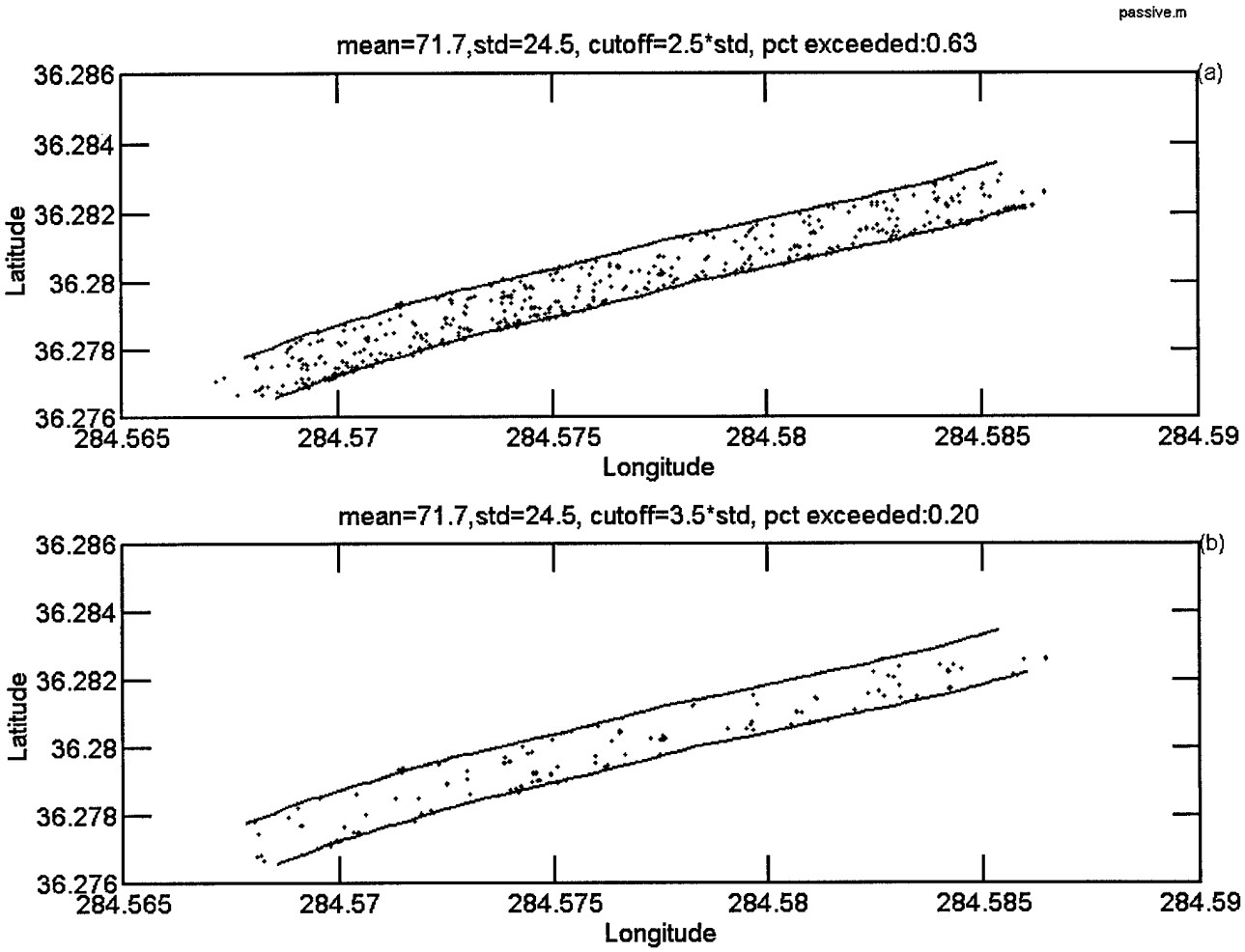

Figure 4. Binary Images Of The Ocean Surface Brightness Derived From The Passive Scanning Measurements. The Corresponding Ocean Surface Topography Is Shown In Figure 3a. The Threshold Is (a) 2.5 Standard Deviations, And (b) 3.5 Standard Deviations Above The Mean.

The binary image of the breaking patches (Figure 4) provides both the statistical average and the distribution pattern of breaking waves in a given area. The image can be further combined with the ocean surface topography (Figure 3a) to yield quantitative information of the breaking distribution with respect to the wave profile. Such information offers a great potential to enhance our understanding of breaking waves in the ocean.

5. SUMMARY AND CONCLUSIONS

The airborne scanning lidar ranging offers a significant capability for a high-resolution mapping of the wave field in the ocean. The resulting two-dimensional images of the ocean surface topography are ideal for the investigation of the wavenumber structure of ocean waves. The concept of applying the airborne spatial wave measurements to derive the source and sink functions in the energy balance equation has been tested with success with scanning radar data (Walsh et al. 1985, 1989; Hwang and Walsh 1998; Hwang et al. 1998). The resolution of the lidar data is at least one order of magnitude better than the radar data, and has been used to calibrate the radar data in the past. High resolution lidar data will extend the wavenumber coverage and increase the measurement precision.

In addition to active ranging, the scanning optical system collects passive images of the surface emissivity and effectively generates instantaneous digitization of the surface brightness condition. The breaking patches show up as bright spots against the dark background of the ambient ocean surface. These images can be used alone or combined with the simultaneously measured surface topography to study the wave breaking processes.

Because airborne systems provide continuous spatial coverage over a large area in a reasonably short time, there is much less variation of the environmental conditions during each flight mission. The quasi-steady conditions simplify significantly the data analysis. In addition to the investigation of the source and sink functions, and the spatial distribution of breaking events, the spatial measurements are also ideal for quantifying the shoaling wave transformation. Finally, the circular scanning measurements can be treated as paired time-lagged or space-lagged data sequences. These time/space lag measurements are suitable for the study of wave statistical properties such as the correlation and coherence functions.

ACKNOWLEDGEMENT

The wind and wave data used in Figures 1 and 2 were obtained from the U. S. Army Field Research Facility web site. The research is supported by the Office of Naval Research (NRL JO 6725-A8 and 7045-A8) and the NASA Office of Earth Science. NRL contribution PP/7332--98-0021.

REFERENCES

Birkemeier, W. A. and E. B. Thornton, 1994: The DUCK94 nearshore field experiment. *Proc. Coast. Dyn. '94*, 815-821.

Birkemeier, W. A., C. E. Long, and K. K. Hathaway, 1996: Delilah, DUCK94, and SandyDuck: Three nearshore field experiments. *Proc. 25th Int. Conf. Coast. Eng.*, **110**, 67-79.

Hoge, F. E., R. N. Swift, and E. B. Frederick, 1980: Water depth measurement using an airborne pulsed neon laser system. *Appl. Opt.*, **19**, 871-887.

Hwang, P. A., and E. J. Walsh, Remote sensing and coastal wave research, *Coastal Dynamics '97*, ed. E. B. Thornton, 337-345, 1998.

Hwang, P. A., E. J. Walsh, W. B. Krabill, R. N. Swift, S. S. Manizade, J. F. Scott, and M. D. Earle, 1998: Airborne remote sensing applications to coastal wave research. *J. Geophys. Res.* (in press).

Krabill, W. B. and C. F. Martin, 1987: Aircraft positioning using global positioning carrier phase data.

Navig., **34**, 1-21.

Krabill, W. B., R. H. Thomas, C. F. Martin, R. N. Swift, and E. B. Frederick, 1995a: Accuracy of airborne laser altimetry over the Greenland ice sheet. *Int. J. Rem. Sens.*, **16**, 1211-1222.

Krabill, W. B., R. H. Thomas, K. Jezek, C. Kuivinen, and S. Manizade, 1995b: Greenland ice sheet thickness changes measured by laser altimetry. *Geophys. Res. Lett.*, **22**, 2341-2344.

Monahan, E. C., 1971: Oceanic whitecaps. *J. Phys. Oceanogr.*, **1**, 139-144.

Monahan, E. C., and I. O'Muircheartaigh, 1980: Optimal power-law description of oceanic whitecap coverage dependence on wind speed. *J. Phys. Oceanogr.*, **10**, 2094-2099.

Phillips, O. M., 1977: *The dynamics of the upper ocean.* 2nd ed., Cambridge Univ. Publ.

Schule, J. J., L. S. Simpson, and P. S. DeLeonibus, 1971: A study of wave spectra with an airborne laser. *J. Geophys. Res.*, **76**, 4160-4171.

Thornton, E. B., and R. T. Guza, 1983: Transformation of wave height distribution. *J. Geophys. Res.*, **88**, 5925-5938.

Walsh, E. J., D. W. Hancock, D. E. Hines, R. N. Swift, and J. F. Scott, 1985: Directional wave spectra measured with the surface contour radar. *J. Phys. Oceanogr.*, **15**, 566-592.

Walsh, E. J., D. W. Hancock, D. E. Hines, R. N. Swift, and J. F. Scott, 1989: An observation of the directional wave spectrum evolution from shoreline to fully developed. *J. Phys. Oceanogr.*, **19**, 670-690.

Wu, J., 1988: Variations of whitecap coverage with wind stress and water temperature. *J. Phys. Oceanogr.*, **18**, 1448-1453.

REPORT DOCUMENTATION PAGE

Form Approved
OBM No. 0704-0188

1. AGENCY USE ONLY *(Leave blank)*	2. REPORT DATE	3. REPORT TYPE AND DATES COVERED
	October 1998	Proceedings

4. TITLE AND SUBTITLE

Airborne Lidar Remote Sensing of Coastal Waves and Breaking Distribution

5. FUNDING NUMBERS

Job Order No. 736725A8

Program Element No.

Project No.

Task No.

Accession No.

6. AUTHOR(S)

Paul A. Hwang, [1]William B. Krabill, Wayne Wright, Edward J. Walsh, and [2]Robert N. Swift

7. PERFORMING ORGANIZATION NAME(S) AND ADDRESS(ES)

Naval Research Laboratory
Oceanography Division
Stennis Space Center, MS 39529-5004

8. PERFORMING ORGANIZATION REPORT NUMBER

NRL/PP/7332--98-0021

9. SPONSORING/MONITORING AGENCY NAME(S) AND ADDRESS(ES)

Office of Naval Research
800 North Quincy Street
Arlington, VA 22217-5000

NASA
Office of Earth Science

10. SPONSORING/MONITORING AGENCY REPORT NUMBER

11. SUPPLEMENTARY NOTES

Proceedings of the Fifth International Conference Remote Sensing for Marine and Coastal Environments, Volume II, 5-7 October 1998, San Diego, CA
[1]NASA/GFSC Laboratory for Hydrospheric Processes, Wallops Island, VA
[2]EG&G Services, Inc., N159, Wallops Flight Facility, Wallops Island, VA

12a. DISTRIBUTION/AVAILABILITY STATEMENT

Approved for public release; distribution is unlimited.

12b. DISTRIBUTION CODE

13. ABSTRACT*(Maximum 200 words)*

A scanning lidar system provides high-resolution two-dimensional measurements of ocean wave displacement. The airborne operation further enhances the speed of data acquisition. These properties allow rapid characterization of the ocean wave environment. In addition to active ranging, the scanning optics can obtain passive measurements of surface emissivity, yielding a digital image of the surface brightness "on the fly." Processed into a binary image, these measurements can provide information on the average statistics and the spatial distribution of breaking waves. Technical specifications of the system and examples of its application are presented.

14. SUBJECT TERMS

remote sensing, coastal waves, airborne scanning lidar, binary images, spatial distribution, and topography

15. NUMBER OF PAGES

5

16. PRICE CODE

17. SECURITY CLASSIFICATION OF REPORT	18. SECURITY CLASSIFICATION OF THIS PAGE	19. SECURITY CLASSIFICATION OF ABSTRACT	20. LIMITATION OF ABSTRACT
Unclassified	Unclassified	Unclassified	SAR